AIDED/AUTOMATIC TARGET DETECTION USING REFLECTIVE HYPERSPECTRAL IMAGERY FOR AIRBORNE APPLICATIONS

December 1998

Hanna T. Haskett
Night Vision & Electronic Sensors Directorate
Ft. Belvoir, VA 22060

Arun K. Sood
George Mason University
Fairfax VA 22030

ABSTRACT

This paper presents an algorithm to support airborne, real-time automatic target detection using combined EO/IR spatial and spectral discriminants for remote sensing surveillance and reconnaissance applications. The algorithm presented in this paper is sufficiently robust and optimized to accommodate high throughput, real-time, sub-pixel, hyperspectral target detection, and can also be used to support man-in-the loop or automatic target detection. The essence of this algorithm is the ability to select the adaptive endmember spectral signatures in real-time, regardless of target, background, and system related effects such as atmospheric conditions, calibration or sensor artifacts. Based on the selected endmembers, the spectral angle of the endmembers is used as the discriminant for target detection or terrain identification. The detection performance and false alarm rate (FAR) including the performances of different combinations of individual bands will be quantified. Statistical analysis including class distributions, various moments of hyperspectral data, and the endmember spectral signatures is examined.

The Forest Radiance I database is collected with the HYDICE hyperspectral sensor (reflective spectral band of 0.4um to 2.5um) at Aberdeen U. S. Army Proving Ground in Maryland. The data set covers an area of about 10km^2.

REPORT DOCUMENTATION PAGE

Form Approved OMB No. 0704-0188

1. REPORT DATE (DD-MM-YYYY)	2. REPORT TYPE	3. DATES COVERED (FROM - TO)
01-12-1998	Conference Proceedings	xx-xx-1998 to xx-xx-1998

4. TITLE AND SUBTITLE	5a. CONTRACT NUMBER
Aided/Automatic Target Detection Using Reflective Hyperspectral Imagery for Airborne Applications Unclassified	5b. GRANT NUMBER 5c. PROGRAM ELEMENT NUMBER
6. AUTHOR(S) Haskett, Hanna T. ; Sood, Arun K. ;	5d. PROJECT NUMBER 5e. TASK NUMBER 5f. WORK UNIT NUMBER
7. PERFORMING ORGANIZATION NAME AND ADDRESS Night Vision & Electronic Sensors Directorate Ft. Belvoir, VA22060	8. PERFORMING ORGANIZATION REPORT NUMBER
9. SPONSORING/MONITORING AGENCY NAME AND ADDRESS Director, CECOM RDEC Night Vision and Electronic Sensors Directorate 10221 Burbeck Road Ft. Belvoir, VA22060-5806	10. SPONSOR/MONITOR'S ACRONYM(S) 11. SPONSOR/MONITOR'S REPORT NUMBER(S)

12. DISTRIBUTION/AVAILABILITY STATEMENT
APUBLIC RELEASE
,

13. SUPPLEMENTARY NOTES
See Also ADM201041, 1998 IRIS Proceedings on CD-ROM.

14. ABSTRACT
This paper presents an algorithm to support airborne, real-time automatic target detection using combined EO/IR spatial and spectral discriminants for remote sensing surveillance and reconnaissance applications. The algorithm presented in this paper is sufficiently robust and optimized to accommodate high throughput, real-time, sub-pixel, hyperspectral target detection, and can also be used to support man-in-the loop or automatic target detection. The essence of this algorithm is the ability to select the adaptive endmember spectral signatures in real-time, regardless of target, background, and system related effects such as atmospheric conditions, calibration or sensor artifacts. Based on the selected endmembers, the spectral angle of the endmembers is used as the discriminant for target detection or terrain identification. The detection performance and false alarm rate (FAR) including the performances of different combinations of individual bands will be quantified. Statistical analysis including class distributions, various moments of hyperspectral data, and the endmember spectral signatures is examined. The Forest Radiance I database is collected with the HYDICE hyperspectral sensor (reflective spectral band of 0.4um to 2.5um) at Aberdeen U. S. Army Proving Ground in Maryland. The data set covers an area of about 10km2.

15. SUBJECT TERMS

16. SECURITY CLASSIFICATION OF:			17. LIMITATION OF ABSTRACT	18. NUMBER OF PAGES	19. NAME OF RESPONSIBLE PERSON
a. REPORT	b. ABSTRACT	c. THIS PAGE	Public Release	18	Fenster, Lynn lfenster@dtic.mil
Unclassified	Unclassified	Unclassified			19b. TELEPHONE NUMBER International Area Code Area Code Telephone Number 703767-9007 DSN 427-9007

1. INTRODUCTION

Previous work shows that spectral signatures of pixels containing a particular material are similar (in shape, but not intensity) throughout an image; and each particular material contained in pixels possesses its own unique and distinguishable spectral signature [1]. This finding shows that spectral information of the hyperspectral data can greatly benefit aided target cueing for airborne applications, due to the uniqueness and consistency of particular spectral signatures. This finding also demonstrates that the spectral signatures of the hyperspectral data are significantly invariant compared to radar signatures [2]. Thus, it is reasonable to expect that spectral information will be as valuable as spatial information in aided target cueing for airborne applications. In conclusion, spectral and spatial information of hyperspectral data can be used individually or together for a variety of aided or automatic detection of real-time applications.

Even with all the benefits of hyperspectral data mentioned above, the high data rate throughput of hyperspectral data containing both spectral and spatial information presents difficulties in real-time detection, especially when used together. The Adaptive Real-Time Endmember Selection and Clutter Suppression (ARES) algorithm [1] significantly reduces the computational complexity even when both spectral and spatial information are used together. The state-of-the-art advancements of the ARES algorithm include the ability to (1) accommodate high-throughput hyperspectral data; (2) select endmember spectral signatures adaptively in real-time; and (3) minimize the effect of variation in sensor calibration, sensor artifacts, and atmospheric conditions. Note that the image distinct elements such as, grass, tree, soil, or target, are often defined as the endmembers in the hyperspectral imagery.

Figure 1 is an example of a single band, 1m Ground Sampling Distance (GSD or footprint), representing the image scene of the hyperspectral imagery used in this paper.

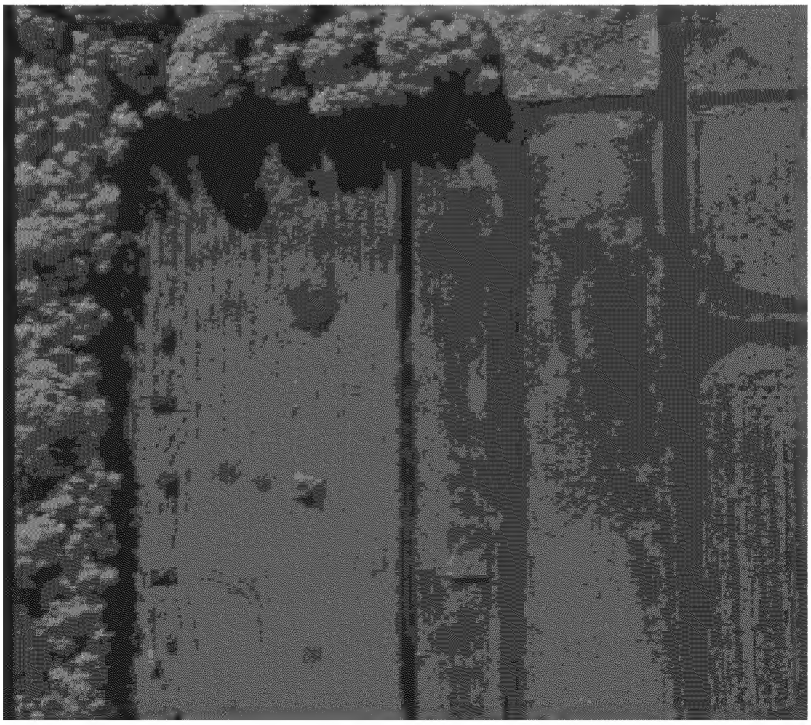

Figure 1: Sample Single Band, 1m GSD Hyperspectral Image

Section 2.0 describes the Forest Radiance I databases and characteristics of the HYDICE sensor. Section 3.0 describes the ARES algorithm. Section 4.0 provides a statistical analysis of the hyperspectral data and selected endmember spectral signatures. The statistical properties of background and targets, including various moments, class distributions, and the physical meaning of the autocorrelation in the spatial domain are also presented. Section 5.0 presents the quantitative detection performance and false alarm rate for different spatial resolutions and times of day [3] and quantifies the detection performance and false alarm rate for different combinations of individual bands for various sets of particular number of bands.

2.0 SENSOR PARAMETERS AND DATABASES

2.1 DATABASES

The research for this paper uses the Forest Radiance I database collected with the HYDICE hyperspectral sensor at Aberdeen U. S. Army Proving Ground in Maryland. The target list of this database consists of several U. S. and foreign vehicles, camouflage nets and panels of different fabrics, and plastic and painted metal decoys. Various camouflage, concealment, and deception scenarios are also included [3]. The Forest Radiance I collection is suitable to be used in evaluations and tests of the hyperspectral data in CC&D scenarios.

A subset of the Forest Radiance I database was utilized for this paper, including scenarios such as targets in the open and at different times of day with footprints of 1m, 2m and 4m. The area coverage of about $10km^2$ and 108 military vehicle targets in this data set are used for detection performance and false alarm rate evaluation.

2.2 SENSOR OVERVIEW

A typical HYDICE hyperspectral imagery cube contains 210 frequency bands (ranging from 0.4μm to 2.5μm) with 320-pixel width, as well as the flight path of the sensor platform making up the height dimension of the scene image, as shown in Figure 2.

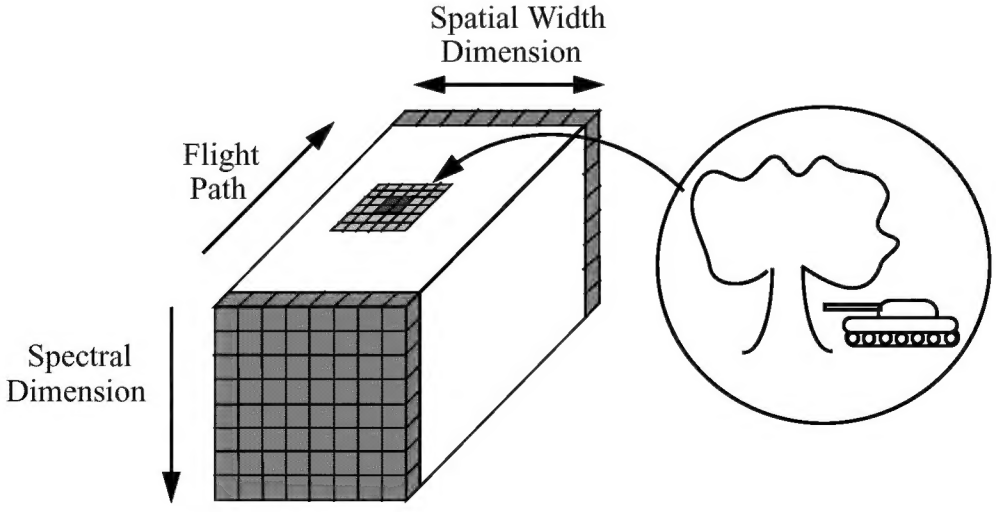

Figure 2: Typical Hyperspectral Data Cube Orientation

2.3 SENSOR SYSTEM DESCRIPTION

The sensor is a nadir-viewing, push-broom, imaging spectroradiometer [3]. The GSD varies from one to four meters as the aircraft's altitude above the ground level (AGL) varies from 6,000 to 20,000 feet. The spectral range of the sensor extends from the visible into the short wave infrared (400 to 2,500 nanometer). The sensor system attributes are shown below [3]:

SYSTEM ATTRIBUTE	SPECIFICATION
Platform	CV-580 Twin Turbo-Prop Aircraft
AGL	2,000 - 7,500m
V/H (aircraft limits)	0.0127 - 0.059 rads/sec
Swath Field of View	8.94^{o}
Swath width	308 pixels
IFOV	0.507 mrad(average)
Array size	320 x 210 pixels
Integration time	1.0 - 42.3 msec
Quantization	12 bits

3.0 DESCRIPTION OF THE ADAPTIVE REAL-TIME ENDMEMBER SELECTION AND CLUTTER SUPPRESSION (ARES) ALGORITHM

3.1 ARES ALGORITHM DESCRIPTION

The ARES algorithm allows the scene to dictate its own endmembers in real-time, which in turn fully represents target and background characteristics. The ARES algorithm is built upon the following assumptions:

1) The spectral signatures of the pixels containing a particular material are similar (in shape, but not intensity) throughout an image,

2) Each particular material contained in any pixel possesses its own unique, distinguishable spectral signature,

3) Natural clutter spectral signatures are distinctively different from man-made material signatures;

4) Natural clutter dominates the majority of the image scene and is limited in variety, such as trees, grass, sand, and water.

5) Edges and shadow spectral shapes are similar to man-made material spectral shapes, as demonstrated in previous work [1] based on the spectral signature analysis of the image elements.

6) The correlations between target and clutter vary more widely than the correlations between clutter types [3].

Based on this, the ARES algorithm was developed [1]. The natural clutter types, which dominate 90% or more of a scene image, are chosen as endmembers. The test pixel is correlated with all the natural clutter endmembers in the scene (as opposed to the targets of interest). Natural clutter is suppressed by the ARES algorithm using the spectral angle discriminator, so only the man-made objects and shadows are left in the image. This presents a significant benefit for subpixel target detection, since the detection appears (by default) in the image by the clutter suppression process. As shadows are highly correlated with man-made materials, small targets effectively become larger [1]. However, shadowed areas of natural backgrounds yield results that would indi-

cate the presence of a man-made object. Note that assumptions 1 to 6 have been demonstrated in the previous work [1, 3] based on the spectral signature analysis of the image elements.

The ARES algorithm consists of two principle processes. Each process is precisely described as follows:

a) Endmember Selection Process:

1) The operator at the ground station or at the sensor platform assesses types of natural clutter in the image scene or terrain. The number of different types of natural clutter in the scene, which is very few (water, sand, tree, grass, bushes), dictate the number of endmembers. The spectral signature of each type of natural clutter is considered an endmember spectral signature. For maximum clutter rejection, all the possible natural clutter types in the scene should be included.

Having the operator at the ground station choose endmembers is used for the target cueing applications. When the ARES algorithm is used as a stand-alone automatic target detection system, all the possible natural clutter types chosen as endmembers can be obtained as the "training" templates in data collection efforts to be stored in the library.

2) In real-time, the spectral signature of pixel locations that contain types of natural clutter are chosen as endmembers from the current sensor scan line (or whenever possible to be obtained). Each endmember is normalized by dividing by its modulus (square root of the sum of the squares of vector components). This particular normalization is essential for the ARES algorithm and is explained in a later section. The set of resulting endmembers is stored (and updated as new types of natural clutter appear in the data) in a library to be used in the clutter rejection process.

3) One of the modulus normalized man-made material spectral signatures is stored in the library initially for the clutter suppression process. This man-made material signature not necessarily that of a target, even a target in the scene, but a man-made material spectral signature from the scene is preferred as this will maximize the natural clutter versus the man-made material separation score. Because obtaining this score (as a discriminant) is important, a man-made material spectral signature must be stored in the library. Again, for cueing applications, in order to obtain the man-made material reference signature in the scene, the operator chooses a pixel from the region where man-made materials are expected to be whenever possible. For stand-alone systems, this man-made material signature can be obtained off-line.

b) Clutter Suppression Process. A normalized Euclidean Inner Product (or dot product) is applied between the test pixel and the endmembers (natural clutter spectral signatures) as well as with a man-made material template. If the maximum score belongs to any one of the natural clutter endmembers, then the test pixel is a non-detection (assigned a zero), otherwise a detection (assigned a one). In other words, if the maximum score does not belong to any of the natural clutter endmembers, then the test pixel is declared as a detection. Since all the natural clutter is highly correlated and dominates most of the scene, the majority of the scene will be blacked out, only a small percentage of man-made materials is left in the image. A simple size filter eliminates most the unwanted man-made objects

(or materials) and a detection of the interested objects (or material) with a particular size is identified. The flow chart for the ARES algorithm is shown in Figure 3.

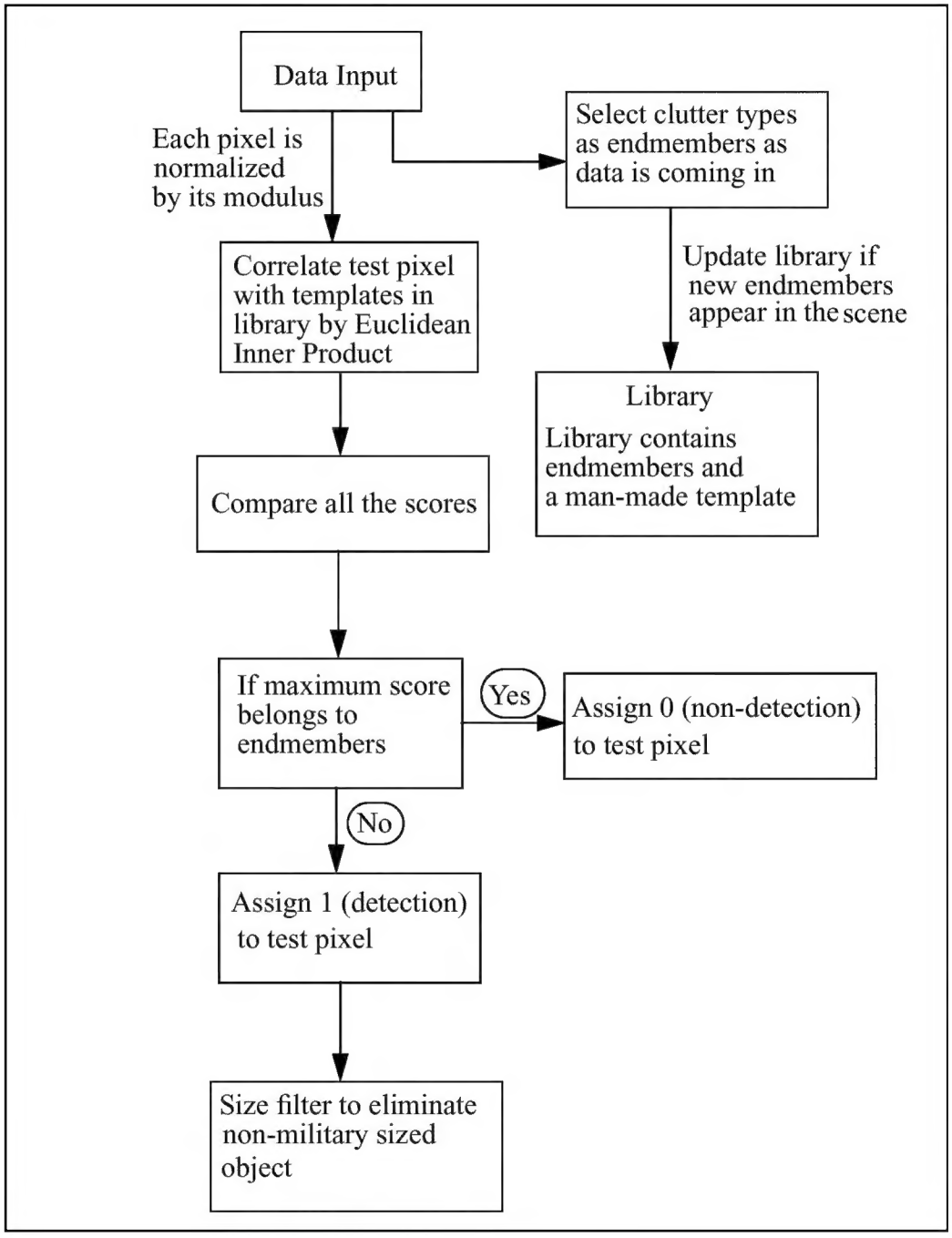

Figure 3: Flow Chart for the ARES Algorithm

3.2 Motivation of Vector Modulus Normalization

This section explains the essential aspects of a particular normalization method required for the ARES algorithm - the vector modulus normalization (square root of the sum of the squares of vector components). The motivation for this particular normalization is based on the fact that magnitudes of spectral signatures of the same image element vary significantly due to the variation of the sun light illumination, while the shapes of the spectral signatures of the same image element remain invariant [1]. To eliminate the magnitude variation effect and only the shapes of the spectral signatures remain, the spectral angle between the spectral signatures are obtained by the normalized correlation method using the Euclidean inner product as discussed below. Also, as long as the vector modulus normalization is taken place, any correlation methods, such as mean square error, variance of error, or cosine of spectral angle produce similar results [1].

The Euclidean inner product can be expressed as

$$\Sigma\alpha\beta = |\alpha||\beta|\cos\theta = (\Sigma\alpha_i^2)^{1/2}(\Sigma\beta_i^2)^{1/2}\cos\theta$$

or

$$\cos\theta = \Sigma\alpha\beta/(\Sigma\alpha_i^2)^{1/2}(\Sigma\beta_i^2)^{1/2} \qquad (1)$$

where α_i and β_i are the ith components of the pattern vectors, and θ is the angle between α and β.

As indicated in Equation (1), each pixel in the image is normalized by its modulus (the square root of the sum of the squares of vector components) to produce a unity amplitude vector, so that when two vectors are performed with the correlation operation, only the angle between two vectors remains to be used as the discriminant. In other words, the smaller the angle, the more similar the shape; the larger the angle, the more different the shape.

When the term $\Sigma\alpha\beta$ is not normalized by $|\alpha|$ and $|\beta|$, the value of $\Sigma\alpha\beta$ is sensitive to three variables: the magnitudes of α and β; and the angle between them (this is why the match filter method is sensitive to the magnitude of the signals). Hence, when the term $\Sigma\alpha\beta$ is normalized by $|\alpha|$ and $|\beta|$, only the angle between α and β is left in Equation (1) as the discrimination factor. Thus, this particular normalization is essential for the ARES algorithm; any other normalization approaches will produce incorrect and unpredictable results. In conclusion, the spectral angle by the modulus-normalized Euclidean inner product (or dot product), rather than the vector projection by the Euclidean inner product, is an appropriate discriminator for the hyperspectral imagery based on the unique characteristics of the spectral signatures (such as consistency in shape, but not in intensity; spectral angles between the clutter and target varied more widely than the spectral angles between the clutter) [1,3]. Also, as the result of the vector modulus normalization, any method of correlations, such as spectral angle, MSE, or VE, produce similar results. However, the spectral angle correlation method is preferred for time-critical target detection applications because it is less computationally intensive than MSE and VE correlation methods.

4.0 STATISTICAL ANALYSIS OF HYPERSPECTRAL DATA

This section contains the statistical analysis of selected endmember spectral signatures and the hyperspectral data used in this paper. The statistical analysis of the hyperspectral data

includes target with clutter and clutter class distributions. The Quantile-Quantile plot (QQ-plot) technique is also employed to check for class distribution similarity with the normally assumed underlying distributions; for example, the target with clutter distribution is usually assumed to be lognormal or normal distribution. The spatial autocorrelation of the region containing only grass or trees in different spectral image planes is also performed. The statistical analysis of the selected endmember and military vehicle target spectral signatures includes the mean and variance in order to show the consistency of the endmember spectral signatures throughout the image. The generation of each graphic illustration is described in detail; and the physical meaning is interpreted in terms of spatial/spectral context when possible.

1. Target and Natural Clutter Endmember Signature Statistical Analysis.

This section illustrates the mean and variance of endmembers (natural clutter) and target spectral signatures. A number of pixels containing only military vehicles, trees or grass are obtained from the image. These pixels are then used to generate the averaged spectral signatures of the endmembers (trees and grass) and military vehicle. As military vehicles are limited in numbers, the number of military vehicle pixels contained in the image is smaller than for grass and trees.

Figure 4 shows typical trees, grass, and military vehicles and their averages. The samples used to determine the averaged signatures for grass, trees, and military vehicle targets consist of 2,000, 700, and 200 pixels respectively. Figures 4(a) and 4(b) show the representative and the averaged spectral signatures of trees. Figures 4(c) and 4(d) show the representative and the averaged spectral signatures of grass. Similarly, Figures 4(e) and 4(f) show the representative and the averaged spectral signatures of military vehicle targets. The variance of each endmember and military target spectral signature (not shown) is very small, compared to the means of their spectral signatures ranging, on the average, from 10^{-5} to 10^{-4}.

Note that the representative spectral signatures are randomly obtained by the method described in the ARES algorithm and are not necessarily contained in the sampled pixels used to determine their means and variances, and the consistency in shapes still remains. This indicates that the spectral signature of each endmember (or target) obtained randomly by the method described in the ARES algorithm is a representative.

Note also that the vertical axis (I) and the horizontal axis (B) in Figure 4 represent the modulus normalized intensity and the number of spectral bands (ranging from 0.4 to 2.5um), respectively.

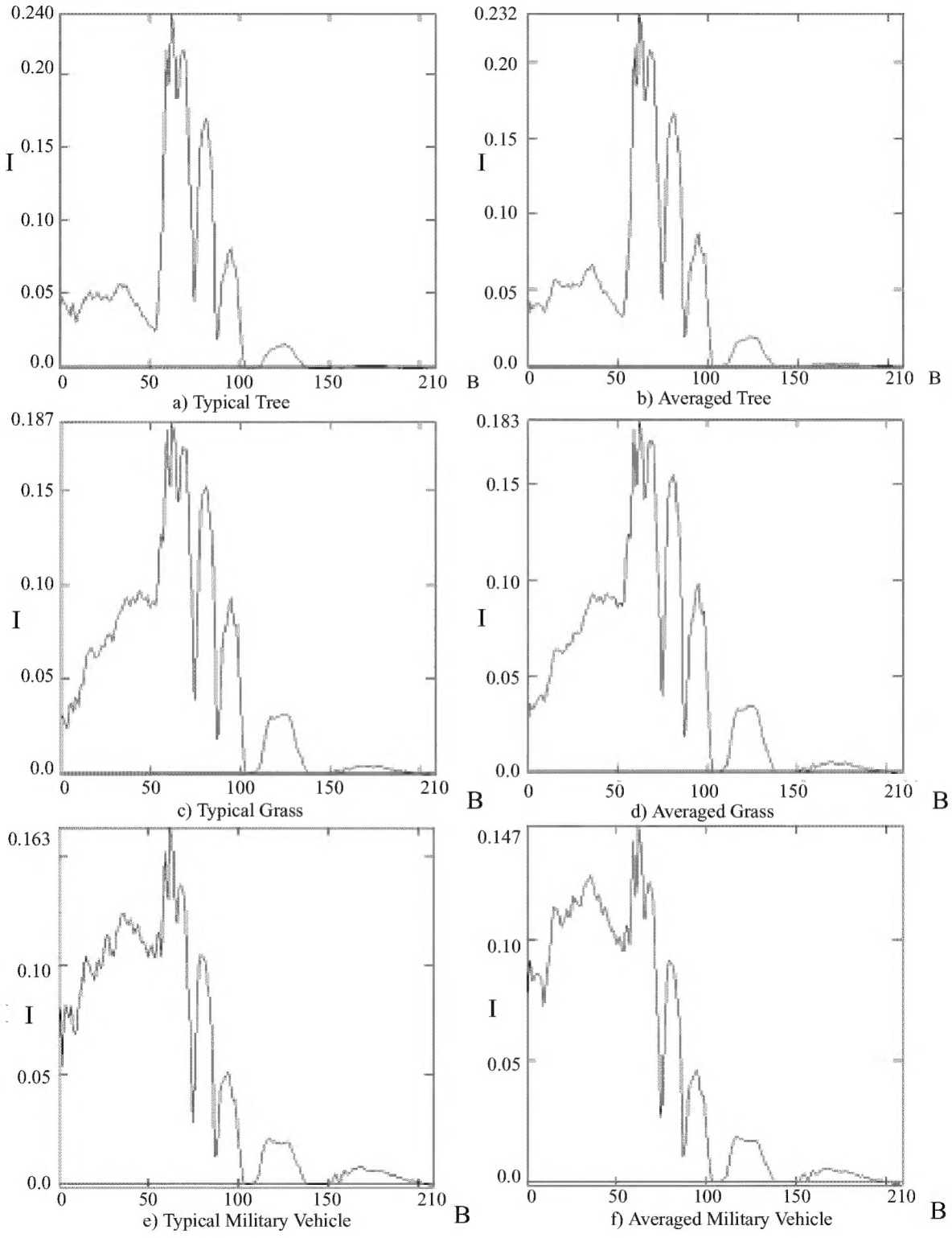

Figure 4. Spectral Signatures of Natural Clutter and Military Target

2. Class Distributions.

This section illustrates and describes the generation of the modulus normalized correlation distributions representing clutter and target with clutter. For simplicity's sake, the modulus normalized correlation is referred to as the correlation throughout this paper.The individual correlation distributions of trees, grass, and military vehicles are also obtained. The generation of correlation or intensity is often used in the statistical classifier approach to obtain class separability. In order to establish class correlation distributions, 2000 pixels of grass, 750 pixels of trees and 200 pixels of military vehicles are extracted from the hyperspectral imagery. Noted that each pixel is a vector representing its spectral signature and is normalized by its vector modulus to produce a unity amplitude vector to avoid the magnitude sensitivity of the match filter effect, as explained in the earlier section of normalization.

For the individual class correlation distributions, each class distribution is generated by correlating each pixel with all the other pixels within each class. For instance, of 2000 grass pixels, the first pixel is correlated with 1,999 pixels, the 2nd pixel is correlated with 1998 pixels, and so on. The individual class correlation values of trees, grass, and military vehicles are close to unity as expected. For presentation purposes, only the class correlation distribution of the military vehicle target along with clutter and target with clutter distributions are illustrated in the same graph of Figure 5. To form the clutter correlation distribution, each of the 750 tree pixels is correlated with the 2000 grass pixels (until all the tree pixels are used).

Similarly, to form the target with clutter correlation distribution, each of 200 military vehicle target pixels is correlated with all the 2000 grass and 750 tree pixels (until all the military vehicle pixels are used). For presentation purposes, all the distributions are normalized by their own maximum values to illustrate the variation in the correlation (horizontal) axis between target and clutter, instead of being normalized by the integrated values under the curve to form the probability density function.

Figure 5 shows, as expected, that (1) the clutter and target with clutter distributions are not as close to unity as the individual distributions; (2) the target with clutter distribution is further to the left of the correlation axis (away from value of 1) than the clutter distribution. The shaded overlapping region between the clutter and target with clutter distributions indicates the false alarm region based on some thresholding (T) of the statistical classifier approach as commonly utilized.

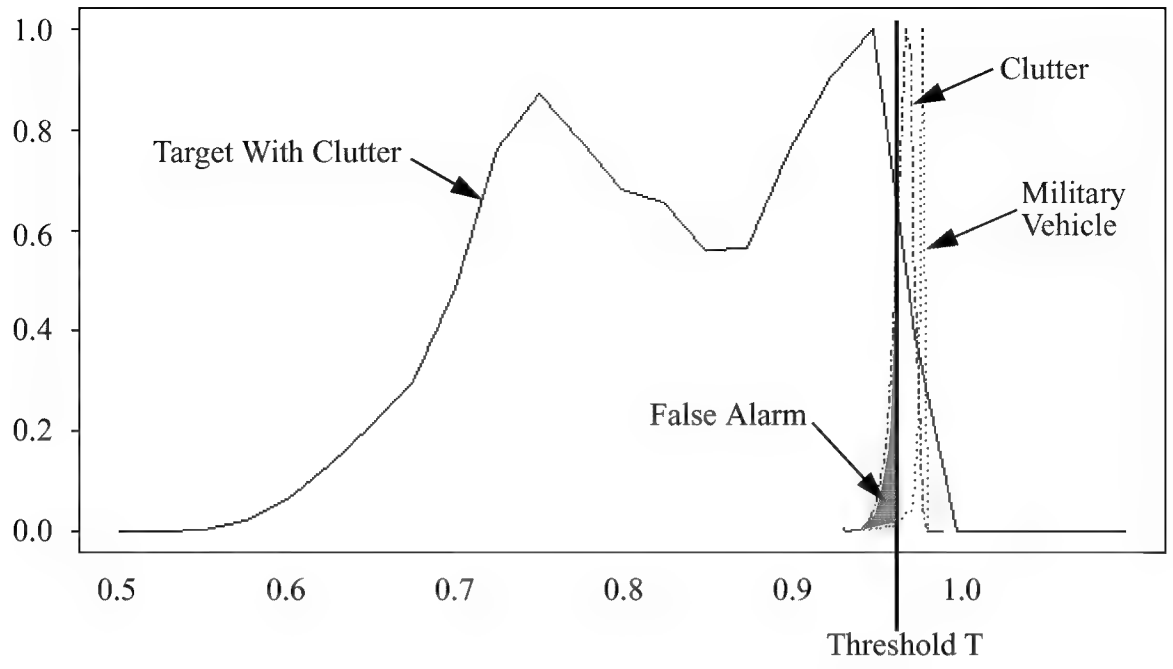

Figure 5. Normalized Correlation (Cosine of Spectral Angle) Distributions of Vehicle Targets, Clutter, and Target With Clutter

As the modulus normalized correlation yields the spectral angle of two vectors, the correlation distributions of the clutter or target with clutter in Figure 5 indicate the following: (1) the spectral angles within each class do not vary significantly; and (2) the spectral angles between target and clutter vary more widely than the spectral angles between the natural clutter types [3].

3. Quantile-Quantile (QQ) Plot.

The QQ-plot is a method used to determine whether a data set has a particular distribution or whether two data sets have the same distribution. The QQ-plot method is a simple technique that plots the sorted values (quantile) of one distribution against the sorted values (quantile) of the other distribution samples. Quantile is a term representing the values of the samples of the distribution. If the distributions are the same, then the QQ-plot will approximate a straight line. If the QQ-plot possesses a "U" shape, then one distribution is skewed relative to the other. An "S" shape means that one distribution has a longer tail than the other [4].

However, third (skewness) and fourth (kurtosis) moments can also be used (but are not recommended due to their sensitivity) to determine the skewness, peakedness, or flatness of data relative to a normal distribution [5]. The QQ-plot in Figure 6 is generated to determine whether the target with clutter distribution belongs to a lognormal or normal distribution, as commonly assumed to model target or background. Figure 6 shows the QQ-plot of the target with clutter distribution (a) against Lognormal and (b) against normal distri-

bution demonstrating that the target with clutter distribution does not have lognormal or normal distributions.

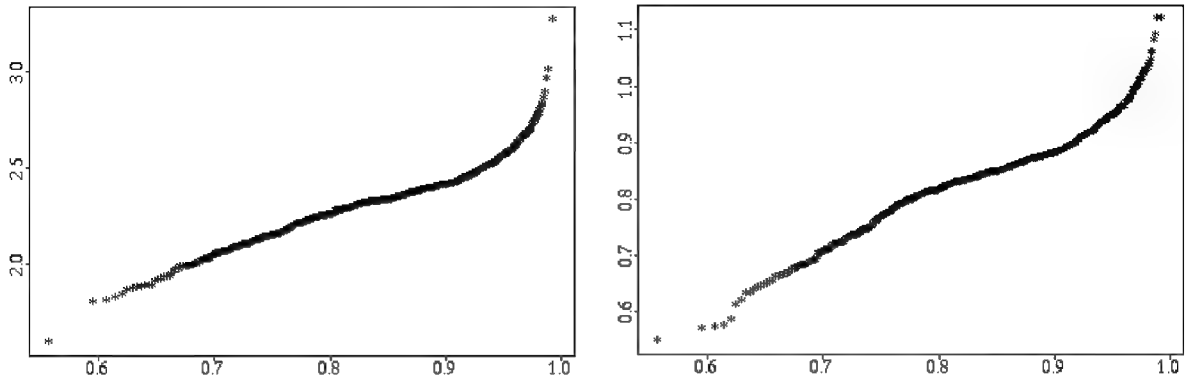

Figure 6. QQ-plot of Target with Clutter distribution of (a)Lognormal; (b)Normal

4. Spatial Autocorrelation.

This section describes the generation of the spatial autocorrelation of the endmembers (grass and trees), and the physical meaning of the data illustrated in Figure 7. Figure 7 shows the autocorrelation of tree and grass regions extracted from different image planes in the hyperspectral imagery. Two different image planes (the 20th and 69th spectral bands) are used in this section. The autocorrelation is defined as follows [6]:

Let $R_i(t)$ be autocorrelation of $n_i(x)$

$$R_i(t) = E[n_i(x)n_i(x+t)] \qquad (2)$$

To perform the autocorrelation operation, a region of the grass and a region of trees in an image of a particular spectral band are extracted. Note that the same regions of grass and trees are extracted from image planes of spectral bands 20 and 69.

The 1-D autocorrelation of the grass (or tree) region is computed by averaging the autocorrelation of the rows containing the grass (or tree) region of a particular image plane. Figure 7(a) shows 1-D autocorrelations of trees and grass regions for the image plane of spectral band 20 to compare the fluctuation and decorrelation between them. Figure 7(b) shows a 1-D autocorrelation of grass alone for the image plane of spectral band 20 at a different scale to show the grass spatial decorrelation. Similarly, Figures 7(c) and 7(d) show 1-D autocorrelations of the grass and trees on the same graph, and 1-D autocorrelation of grass alone, respectively for the image plane of spectral band 69. Note that the autocorrelation in Figure 7 is normalized by $E[n_0(x)n_0(x)]$, simply for the presentation and interpretation purposes. The vertical (R) axis represents the autocorrelation and the horizontal (N) axis represents the number of pixels.

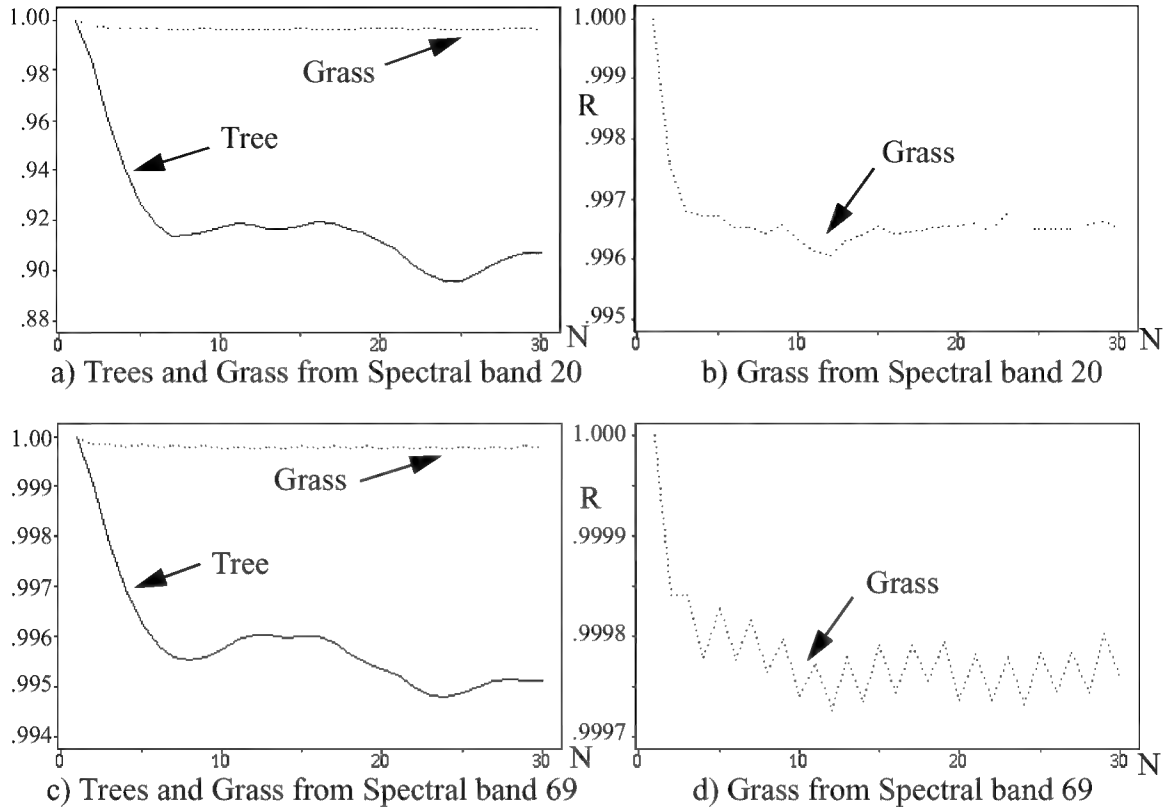

Figure 7: 1-D Autocorrelation of a Typical Row of Natural Clutter in a Single-Band Image Plane of the Hyperspectral Imagery.

The gradual (or abrupt) drop in the vertical direction of the autocorrelation illustrates how slowly (or fast) the grass and tree become decorrelated in the spatial domain. The variation in the horizontal direction of the autocorrelation shows the consistency of the pixel value contained in the region. The physical decorrelation can be interpreted in a distance metric unit, such as meter or foot, depending on the footprint of the pixel size. For instance, the pixel size of the data used in Figure 7 is 1m X 1m. The tree decorrelates faster before 5 meters and slower after 5 meters consistently in both image planes of spectral bands 20 and 69. Figures 7(a) and 7(b) show that grass decorrelates faster than trees since the grass drops more abruptly than the trees, but less overall, in the vertical direction. In Figure 7(a), grass shows less variation than trees in the horizontal direction. This indicates that grass is more consistent than trees from pixel to pixel, as expected, as trees present more texture and variation than grass in an image. Figures 7(c) and 7(d) show a similar effect; however, there are some pattern fluctuation in grass pixels for spectral band 69. Figure 7(d) shows an example of pattern noise or sensor artifacts contained in the hyperspectral imagery.

5.0 DETECTION PERFORMANCE AND FALSE ALARM RATE

This section, for comparison purposes, 1) presents the quantitative detection performance and false alarm rate for different ground sampling distances (GSD or footprints) of various sun angles; and 2) quantifies the detection performance and false alarm rate for different combinations of individual bands for various sets of the particular number of bands using the ARES algorithm.

The typical definitions for probability of detection (Pd) and false alarm rate (FAR) are as follows:
Probability of Detection: The number of correctly detected targets out of the groundtruthed target opportunity for detection where the groundtruthed target is defined as a target of known location and type in an image.

Pd = (number of targets detected)/(number of targets in the set or subset)

False Alarm Rate: The number of false alarms per unit area coverage. A false alarm is defined to be a decision output produced by the algorithm that does not correspond with a ground truth opportunity.

FAR = (number of false alarms)/(area coverage in the data set)

There are 108 target opportunities, and the area coverage is approximately 10 km^2. The target list contained in this data set consists of a variety of man-made objects such as, camouflage nets, panels, and military vehicles; only military vehicles are considered as target opportunities to be detected in this performance evaluation.

5.1 Detection Performance and FAR for different GSD's.

Table 1 shows the detection performance and FAR for different GSD's at different times of day. The overall performance is also presented for each GSD of 1m, 2m, and 4m [3].

Table 1. Detection Performance and False Alarm Rate of Different GSD's [3]

Time of Day / GSD	De-tec-tions	Target Opport-unities	False Alarms	Area Coverage (km^2)	Pd	FAR (FA/km^2)	Pd	FA per Sq.Km.
AM 1mX1m	14	18	18	.41	.78	44	.83	34
PM 1mX1m	16	18	10	.41	.89	24		
AM 2mX2m	14	18	34	.82	.78	41	.78	52
PM 2mX2m	14	18	72	1.23	.78	59		
AM 4mX4m	9	18	315	3.28	.50	96	.56	96
PM 4mX4m	11	18	318	3.28	.61	97		

5.2 Detection Performance and FAR for Different Combinations of Individual Bands.

Figures 8 (a) through (h) show Pd and FAR performances for 1 meter ground sampling distance (GSD) using different combinations of individual, narrow bands (chosen within the 210 band signatures). The number of bands are 3, 6, 10, 20, 60, 90, 120, and 150.

Obviously, it is difficult to obtain performances for all the combinations of individual bands. For each different number of bands, 7 to 9 different sets of bands were used and the results are shown in Figures 8(a) through (h). The original spectral signatures extending from .4 to 2.5 um contain 210 bands are divided into 3 spectral regions corresponding to visible (.4-.7um) containing 56 narrow bands, near infrared (.7-1.0um) containing 24 bands, and short wave infrared (1.0-2.5um) containing 130 bands. The individual bands were divided between these three regions as equally as possible. Within each region the individual bands were chosen in a semi-arbitrary fashion.

For instance, Figure 8(a) shows performances of different combinations of 3 individual bands. Each combination of 3 individual bands consists of one band from each region of visible, near infrared, and shortwave infrared, respectively.

As shown in Figure 8(a) through (h), performances are comparable whether a few bands or tens of bands are used. In other words, a few bands or tens of bands can obtain the same performance (given that those particular bands are known as a priori). Figure 8 also reinforces the finding that hundreds of bands do not necessarily provide better performance than tens of bands which was demonstrated in the previous work [7].

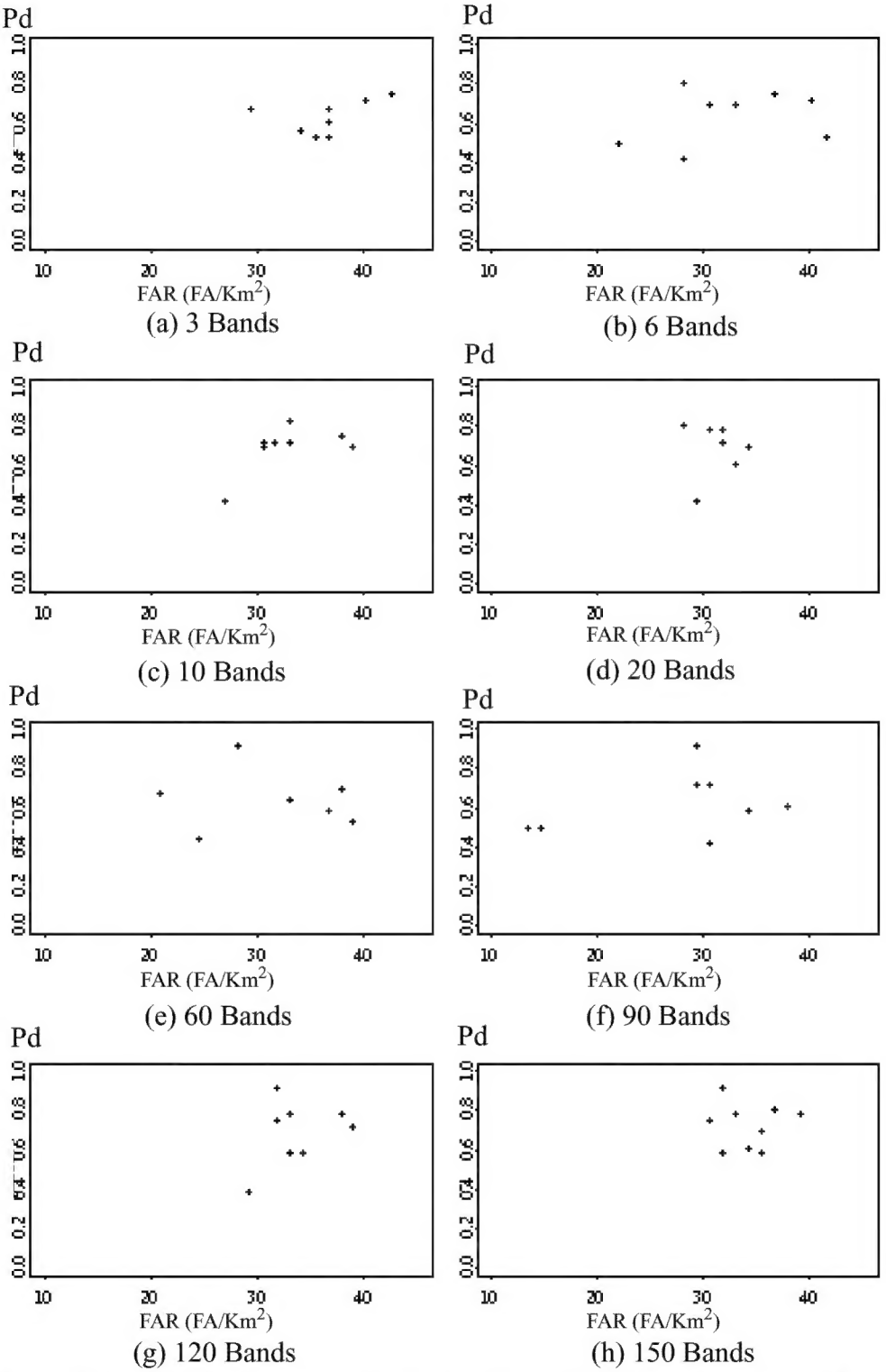

Figure 8. 1m GSD Performance of Individual Bands for Different Numbers of Bands

6. CONCLUSION

The clutter background in infrared single-band images has posed difficult problems for automatic target detection/recognition, especially for low spatial resolution targets (or sub-pixel targets). Hyperspectral imagery offers another dimension of information. It has been established that the hyperspectral imagery has the following properties [1]: (1) The spectral signatures of each image element are consistently similar (in shape, not intensity) throughout the image scene; (2) Each image element possesses its own unique, distinguishable spectral signature; (3) Natural clutter types are highly correlated with each other, likewise for man-made materials, yet natural clutter and man-made materials are highly uncorrelated; (4) Edges and shadow spectral signatures are similar to man-made material spectral signatures. (5) The spectral signatures remain unique within a given footprint size, but differ somewhat from the same signatures collected with pixel footprints of different sizes. The consistency, uniqueness, and distinctiveness of any particular material regardless of atmospheric conditions, calibrations or sensor artifacts can be explained. Any disturbance caused by atmospheric conditions is carried and included in all the signatures for all materials or objects in the image. Hence, all spectral signatures carry the same disturbance. In addition, the spectral angles within each class do not vary significantly. The spectral angles between target and clutter vary more widely than the spectral angles between clutter types. Based on these findings, the ARES algorithm was developed. ARES offers a robust technique that can accommodate high throughput, real-time, hyperspectral data for target detection. These findings also indicate that the spectral signatures produced by a hyperspectral system can be used to identify particular materials with man-in-the-loop or aided target detection due to their uniqueness and distinctiveness throughout an image.

ACKNOWLEDGEMENT

Authors would like to thank Dr. Don Reago and Dr. Tom Witten at Night Vision and Electronic Sensors Directorate for their insightful comments, and discussions. Authors would also like to thank Spectral Information Technology Application Center for providing the data.

REFERENCES

[1] H. T. Haskett and A. K. Sood, "An Adaptive Real-Time Endmember Selection Algorithm for Sub-Pixel Target Detection Using Hyperspectral Data", Proceedings of the 1997 IRIS Specialty Group on Camouflage, Concealment and Deception, October 1997.

[2] M. Gahler and H. Tran,"Survey of Millimeter-Wave Radar Algorithm for Stationary Target Recognition", Night Vision Lab, Ft. Belvoir, Dec 1991.

[3] H. T. Haskett and A. K. Sood, "Spectral-Spatial Automatic Target Detection using Hyperspectral Data", Proceedings of International Symposium on Spectral Sensing Research, Dec. 1997.

[4] StatSci, S-PLUS Reference Manual. Statistical Sciences, Inc. Seattle, Washington, Sept. 1991.

[5] W. H. Press, et. al., Numerical Recipes in C. Cambridge University Press, 1988.

[6] V. A. Topkar and A. K. Sood, "Statistical Analysis of Scale Space", IEEE Signal Processing, Vol. 26, 1992, pp.307-334.

[7] H. T. Haskett and A. K. Sood, "Trade-off studies of detection performance versus the number of reflective spectral bands in hyperspectral imagery", Proceedings of SPIE on Algorithms for Multispectral and Hyperspectral Imagery IV, Orlando FL, April 1998.
[8] A. K. Jain, Fundamentals of Digital Image Processing. Prentice-Hall Inc., 1989.
[9] K. Fukunaga, Introduction to Statistical Pattern Recognition. Academic Press, 1972.